



**HAL**  
open science

## **In vivo structural imaging of the cornea by polarization-resolved second harmonic microscopy.**

Gaël Latour, Ivan Gusachenko, Laura Kowalczuk, Isabelle Lamarre,  
Marie-Claire Schanne-Klein

### ► **To cite this version:**

Gaël Latour, Ivan Gusachenko, Laura Kowalczuk, Isabelle Lamarre, Marie-Claire Schanne-Klein. In vivo structural imaging of the cornea by polarization-resolved second harmonic microscopy.. *Biomedical optics express*, 2012, 3 (1), pp.1-15. 10.1364/BOE.3.000001 . hal-00324465

**HAL Id: hal-00324465**

**<https://hal.science/hal-00324465>**

Submitted on 20 Nov 2013

**HAL** is a multi-disciplinary open access archive for the deposit and dissemination of scientific research documents, whether they are published or not. The documents may come from teaching and research institutions in France or abroad, or from public or private research centers.

L'archive ouverte pluridisciplinaire **HAL**, est destinée au dépôt et à la diffusion de documents scientifiques de niveau recherche, publiés ou non, émanant des établissements d'enseignement et de recherche français ou étrangers, des laboratoires publics ou privés.

# *In vivo* structural imaging of the cornea by polarization-resolved second harmonic microscopy

Gaël Latour,<sup>1</sup> Ivan Gusachenko,<sup>1</sup> Laura Kowalczyk,<sup>2</sup> Isabelle Lamarre,<sup>1</sup> and Marie-Claire Schanne-Klein<sup>1,\*</sup>

<sup>1</sup>Laboratory for Optics and Biosciences, École Polytechnique—CNRS—INSERM, 91128 Palaiseau, France

<sup>2</sup>Laboratory for Applied Optics, ENSTA ParisTech—École Polytechnique—CNRS, 91761 Palaiseau, France

\*marie-claire.schanne-klein@polytechnique.edu

**Abstract:** The transparency and mechanical strength of the cornea are related to the highly organized three-dimensional distribution of collagen fibrils. It is of great interest to develop specific and contrasted *in vivo* imaging tools to probe these collagenous structures, which is not available yet. Second Harmonic Generation (SHG) microscopy is a unique tool to reveal fibrillar collagen within unstained tissues, but backward SHG images of cornea fail to reveal any spatial features due to the nanometric diameter of stromal collagen fibrils. To overcome this limitation, we performed polarization-resolved SHG imaging, which is highly sensitive to the sub-micrometer distribution of anisotropic structures. Using advanced data processing, we successfully retrieved the orientation of the collagenous fibrils at each depth of human corneas, even in backward SHG homogenous images. Quantitative information was also obtained about the submicrometer heterogeneities of the fibrillar collagen distribution by measuring the SHG anisotropy. All these results were consistent with numerical simulation of the polarization-resolved SHG response of cornea. Finally, we performed *in vivo* SHG imaging of rat corneas and achieved structural imaging of corneal stroma without any labeling. Epi-detected polarization-resolved SHG imaging should extend to other organs and become a new diagnosis tool for collagen remodeling.

© 2011 Optical Society of America

**OCIS codes:** (180.4315) Nonlinear microscopy; (120.5410) Polarimetry; (190.4160) Multiharmonic generation; (170.3880) Medical and biological imaging; (170.4470) Ophthalmology.

## References and links

1. R. F. Guthoff, A. Zhivov, and O. Stachs, "In vivo confocal microscopy, an inner vision of the cornea - a major review," *Clin. Experiment. Ophthalmol.* **37**(1), 100–117 (2009).
2. M. Gora, K. Karnowski, M. Szkulmowski, B. J. Kaluzny, R. Huber, A. Kowalczyk, and M. Wojtkowski, "Ultra high-speed swept source OCT imaging of the anterior segment of human eye at 200 kHz with adjustable imaging range," *Opt. Express* **17**(17), 14880–14894 (2009).
3. G. Latour, G. Georges, L. S. Lamoine, C. Deumié, J. Conrath, and L. Hoffart, "Human graft cornea and laser incisions imaging with micrometer scale resolution full-field optical coherence tomography," *J. Biomed. Opt.* **15**(5), 056006 (2010).
4. J. H. Krachmer, M. J. Mannis, and E. J. Holland, *Cornea*, 2nd ed. (Mosby, 2005).
5. K. Plamann, F. Aptel, C. L. Arnold, A. Courjaud, C. Crotti, F. Deloison, F. Druon, P. Georges, M. Hanna, J.-M. Legeais, F. Morin, É. Mottay, V. Nuzzo, D. A. Peyrot, and M. Savoldelli, "Ultrashort pulse laser surgery of the cornea and the sclera," *J. Opt.* **12**(8), 084002 (2010).
6. M. Hao, K. Flynn, C. Nien-Shy, B. E. Jester, M. Winkler, D. J. Brown, O. La Schiazza, J. Bille, and J. V. Jester, "In vivo non-linear optical (NLO) imaging in live rabbit eyes using the Heidelberg Two-Photon Laser Ophthalmoscope," *Exp. Eye Res.* **91**(2), 308–314 (2010).
7. P. J. Campagnola, A. C. Millard, M. Terasaki, P. E. Hoppe, C. J. Malone, and W. A. Mohler, "Three-dimensional high-resolution second-harmonic generation imaging of endogenous structural proteins in biological tissues," *Biophys. J.* **82**(1), 493–508 (2002).

8. W. R. Zipfel, R. M. Williams, R. Christie, A. Y. Nikitin, B. T. Hyman, and W. W. Webb, "Live tissue intrinsic emission microscopy using multiphoton-excited native fluorescence and second harmonic generation," *Proc. Natl. Acad. Sci. U.S.A.* **100**(12), 7075–7080 (2003).
9. D. W. Piston, B. R. Masters, and W. W. Webb, "Three-dimensionally resolved NAD(P)H cellular metabolic redox imaging of the in situ cornea with two-photon excitation laser scanning microscopy," *J. Microsc.* **178**(1), 20–27 (1995).
10. A. T. Yeh, N. Nassif, A. Zoumi, and B. J. Tromberg, "Selective corneal imaging using combined second-harmonic generation and two-photon excited fluorescence," *Opt. Lett.* **27**(23), 2082–2084 (2002).
11. M. Han, G. Giese, and J. Bille, "Second harmonic generation imaging of collagen fibrils in cornea and sclera," *Opt. Express* **13**(15), 5791–5797 (2005).
12. S.-W. Teng, H.-Y. Tan, J.-L. Peng, H.-H. Lin, K. H. Kim, W. Lo, Y. Sun, W.-C. Lin, S.-J. Lin, S.-H. Jee, P. T. C. So, and C.-Y. Dong, "Multiphoton autofluorescence and second-harmonic generation imaging of the ex vivo porcine eye," *Invest. Ophthalmol. Vis. Sci.* **47**(3), 1216–1224 (2006).
13. N. Morishige, T. Nishida, and J. J. Jester, "Second harmonic generation for visualizing 3-dimensional structure of corneal collagen lamellae," *Cornea* **28**(Suppl 1), S46–S53 (2009).
14. P. Matteini, F. Ratto, F. Rossi, R. Cicchi, C. Stringari, D. Kapsokalyvas, F. S. Pavone, and R. Pini, "Photothermally-induced disordered patterns of corneal collagen revealed by SHG imaging," *Opt. Express* **17**(6), 4868–4878 (2009).
15. F. Aptel, N. Olivier, A. Deniset-Besseau, J.-M. Legeais, K. Plamann, M.-C. Schanne-Klein, and E. Beaurepaire, "Multimodal nonlinear imaging of the human cornea," *Invest. Ophthalmol. Vis. Sci.* **51**(5), 2459–2465 (2010).
16. N. Olivier, F. Aptel, K. Plamann, M.-C. Schanne-Klein, and E. Beaurepaire, "Harmonic microscopy of isotropic and anisotropic microstructure of the human cornea," *Opt. Express* **18**(5), 5028–5040 (2010).
17. J. M. Bueno, E. J. Gualda, A. Giakoumaki, P. Pérez-Merino, S. Marcos, and P. Artal, "Multiphoton microscopy of ex vivo corneas after collagen cross-linking," *Invest. Ophthalmol. Vis. Sci.* **52**(8), 5325–5331 (2011).
18. M. Strupler, A.-M. Pena, M. Herness, P.-L. Tharax, J.-L. Martin, E. Beaurepaire, and M.-C. Schanne-Klein, "Second harmonic imaging and scoring of collagen in fibrotic tissues," *Opt. Express* **15**(7), 4054–4065 (2007).
19. A. Deniset-Besseau, J. Duboisset, E. Benichou, F. Hache, P.-F. Brevet, and M.-C. Schanne-Klein, "Measurement of the second-order hyperpolarizability of the collagen triple helix and determination of its physical origin," *J. Phys. Chem. B* **113**(40), 13437–13445 (2009).
20. R. Lacombe, O. Nadiarnykh, S. S. Townsend, and P. J. Campagnola, "Phase Matching considerations in Second Harmonic Generation from tissues: Effects on emission directionality, conversion efficiency and observed morphology," *Opt. Commun.* **281**(7), 1823–1832 (2008).
21. M. Strupler and M.-C. Schanne-Klein, "Simulating second harmonic generation from tendon—do we see fibrils?" in *Biomedical Optics*, OSA Technical Digest (CD) (Optical Society of America, 2010), paper BTuD83.
22. M. Rivard, M. Laliberté, A. Bertrand-Grenier, C. Harnagea, C. P. Pfeffer, M. Vallières, Y. St-Pierre, A. Pignolet, M. A. El Khakani, and F. Légaré, "The structural origin of second harmonic generation in fascia," *Biomed. Opt. Express* **2**(1), 26–36 (2011).
23. F. Tiaho, G. Recher, and D. Rouède, "Estimation of helical angles of myosin and collagen by second harmonic generation imaging microscopy," *Opt. Express* **15**(19), 12286–12295 (2007).
24. P. Stoller, K. M. Reiser, P. M. Celliers, and A. M. Rubenchik, "Polarization-modulated second harmonic generation in collagen," *Biophys. J.* **82**(6), 3330–3342 (2002).
25. O. Nadiarnykh and P. J. Campagnola, "Retention of polarization signatures in SHG microscopy of scattering tissues through optical clearing," *Opt. Express* **17**(7), 5794–5806 (2009).
26. I. Gusachenko, G. Latour, and M.-C. Schanne-Klein, "Polarization-resolved Second Harmonic microscopy in anisotropic thick tissues," *Opt. Express* **18**(18), 19339–19352 (2010).
27. S. Brasselet, D. Ait-Belkacem, A. Gasecka, F. Munhoz, S. Brustlein, and S. Brasselet, "Influence of birefringence on polarization resolved nonlinear microscopy and collagen SHG structural imaging," *Opt. Express* **18**(14), 14859–14870 (2010).
28. S. Psilodimitrakopoulos, S. I. C. O. Santos, I. Amat-Roldan, A. K. N. Thayil, D. Artigas, and P. Loza-Alvarez, "In vivo, pixel-resolution mapping of thick filaments' orientation in nonfibrillar muscle using polarization-sensitive second harmonic generation microscopy," *J. Biomed. Opt.* **14**(1), 014001 (2009).
29. W.-L. Chen, T.-H. Li, P.-J. Su, C.-K. Chou, P. T. Fwu, S.-J. Lin, D. Kim, P. T. C. So, and C.-Y. Dong, "Second harmonic generation chi tensor microscopy for tissue imaging," *Appl. Phys. Lett.* **94**(18), 183902 (2009).
30. V. Nucciotti, C. Stringari, L. Sacconi, F. Vanzi, L. Fusi, M. Linari, G. Piazzesi, V. Lombardi, and F. S. Pavone, "Probing myosin structural conformation in vivo by second-harmonic generation microscopy," *Proc. Natl. Acad. Sci. U.S.A.* **107**(17), 7763–7768 (2010).
31. S. V. Plotnikov, A. C. Millard, P. J. Campagnola, and W. A. Mohler, "Characterization of the myosin-based source for second-harmonic generation from muscle sarcomeres," *Biophys. J.* **90**(2), 693–703 (2006).
32. E. E. B. A. Directory, 18th ed. (European Eye Bank Association, 2010).
33. P. Réfrégier, M. Roche, and S. Brasselet, "Precision analysis in polarization-resolved second harmonic generation microscopy," *Opt. Lett.* **36**(11), 2149–2151 (2011).
34. J. C. Mansfield, C. P. Winlove, J. Moger, and S. J. Matcher, "Collagen fiber arrangement in normal and diseased cartilage studied by polarization sensitive nonlinear microscopy," *J. Biomed. Opt.* **13**(4), 044020 (2008).
35. L. J. Bour, "Polarized light and the eye" in *Visual Optics and Instrumentation*, W. N. Charman, ed. (CRC Press, 1991), Vol. 1, Chap. 13.
36. L. Novotny and B. Hecht, *Principles of Nano-Optics* (Cambridge University Press, 2006).
37. W. Radner, M. Zehetmayer, R. Aufreiter, and R. Mallinger, "Interlacing and cross-angle distribution of collagen lamellae in the human cornea," *Cornea* **17**(5), 537–543 (1998).

## 1. Introduction

The cornea is the outer part of the eye that protects against external injuries and contributes to 2/3 to the eye refractive power. Commercially available techniques, such as confocal reflectance microscopy [1] or optical coherence tomography (OCT) [2,3], enable three-dimensional (3D) cell-scale imaging of cornea. However, these techniques lack specificity or contrast when looking at the collagen organization of the corneal stroma. The stroma represents 90% of the corneal thickness and is composed of more than 250 stacked collagen lamellae that are 1-3  $\mu\text{m}$  thick [4]. Each lamella forms 10-100  $\mu\text{m}$  wide domains that are comprised of 30 nm diameter collagen fibrils organized into a hexagonal lattice. This highly organized structure is responsible for both the transparency and the mechanical strength of the cornea. It may be disrupted in case of a variety of injuries and pathologies (e.g. keratoconus) [4] or after laser surgery [5]. It is therefore of great interest to develop *in vivo* imaging techniques that provide structural and quantitative information about the corneal stroma.

Multiphoton microscopy (MPM) has been shown to enable 3D imaging of biological tissues with similar resolution as the other optical techniques mentioned above. Strong two-photon excited fluorescence (2PEF) signals can be obtained from exogenous labels and *in vivo* tracking of fluorescent microspheres was recently reported in rabbit corneas [6]. However, it is of great interest to take advantage of endogenous MPM signals to image *unstained* corneas [7,8]. MPM has been shown to provide *ex vivo* specific and contrasted images of unstained corneas by using Second Harmonic Generation (SHG) and Third Harmonic Generation (THG) signals to complement usual 2PEF signals [9–17]. THG signals are related to micrometer-sized optical heterogeneities and are obtained at the lamellar interfaces [16]. However, THG signals are mainly detected in the forward direction, which is not appropriate for *in vivo* imaging. SHG is a coherent second order nonlinear signal that probes dense non-centrosymmetrical macromolecular structures such as fibrillar collagen [7,8,18,19]. Since the diameter of stromal collagen fibrils is much smaller than the optical resolution, collagen fibrils are not resolved in the SHG images of cornea. Accordingly, backward SHG (B-SHG) images can be considered as nearly homogeneous with speckle-like background at the micrometer scale [11,13,15]. However, forward SHG (F-SHG) images exhibit striated features that are attributed to complex coherent processes within the focal volume with different phase-matching conditions than in the B-SHG images [20–22]. These striated features are generally considered to indicate the orientation of the lamellar domains [11,13,15,16]. Therefore, SHG microscopy has been mainly limited to forward imaging in excised corneas up until now, since only F-SHG images seem to provide information about the stromal architecture. Application of THG or SHG microscopy to *in vivo* imaging may take advantage of internal reflections at the eye optical interfaces to image forward-radiated signals in an epi-configuration; however, these back-scattered signals are quite low and direct utilization of B-SHG signals is the most promising technique for *in vivo* imaging.

This work aims to implement polarization-resolved B-SHG microscopy to retrieve orientation information about the 30 nm-diameter stromal collagen fibrils and to enable *in vivo* structural imaging of cornea without any labeling. Polarization resolved techniques are indeed highly sensitive to the sub-micrometer distribution of anisotropic elementary components within a sample, much below the optical resolution, as routinely exploited in ellipsometry measurements. Polarization-resolved SHG microscopy was first developed in rat-tail tendons [23–27] and in skeletal muscle [25,28–31] to determine orientation maps. It was also used in *ex vivo* corneas using a forward detection configuration to study thermal disruption of the collagen lamellae [14]. However, polarization-resolved SHG microscopy was never used to visualize the 3D organization of nanometer-sized fibrils in an epi-configuration until now.

The paper is organized as follows; we first introduce experimental implementation of polarization-resolved SHG and theoretical background based on tensorial formalism of nonlinear optics. We also perform numerical simulations to understand the construction of the polarization-resolved SHG signals from stacked adjacent lamellae. We then show that this method successfully retrieves the orientation and anisotropy of the collagenous lamellar domains in human excised corneas both from F-SHG and B-SHG signals. Most importantly, we perform *in vivo* polarization-resolved SHG imaging of rat corneas and demonstrate that our method also applies to that configuration. Finally, we discuss the robustness and interest of this approach and we propose further *in vivo* studies.

## 2. Materials and methods

### 2.1. Polarization-resolved SHG microscopy

MPM imaging was performed using a custom-built laser scanning upright microscope, based on a femtosecond titanium-sapphire laser (Tsunami, Spectra-Physics) and photon-counting detection (P25PC photomultiplier tubes, Electron Tubes) [15,18,26] (Fig. 1A). High numerical aperture water immersion objectives (20x, NA 0.95 or 60x, NA 1.2, Olympus) were used to achieve lateral and axial spatial resolutions of  $0.4 \times 1.6$  or  $0.3 \times 0.9 \mu\text{m}^2$  at 860 nm near the sample surface. B-SHG and 2PEF signals were detected in the backward direction for *in vivo* imaging, while in *ex vivo* corneas, F-SHG signals were also collected. We used suitable spectral filters to reject the excitation laser beam (FF01-680/SP and FF01-720/SP, Semrock), and select the 2PEF emission (GG455 and GG400 high-pass filters at 730 and 860 nm respectively, Schott) or the SHG signal (Hg01-365 and FF01-427/10 interferential filters respectively, Semrock). Multimodal image stacks were recorded using 200 to 300 kHz pixel rate with 0.5 to 0.8  $\mu\text{m}$  pixel size, and 0.5  $\mu\text{m}$  (fine lamellar studies) to 10  $\mu\text{m}$  (structural

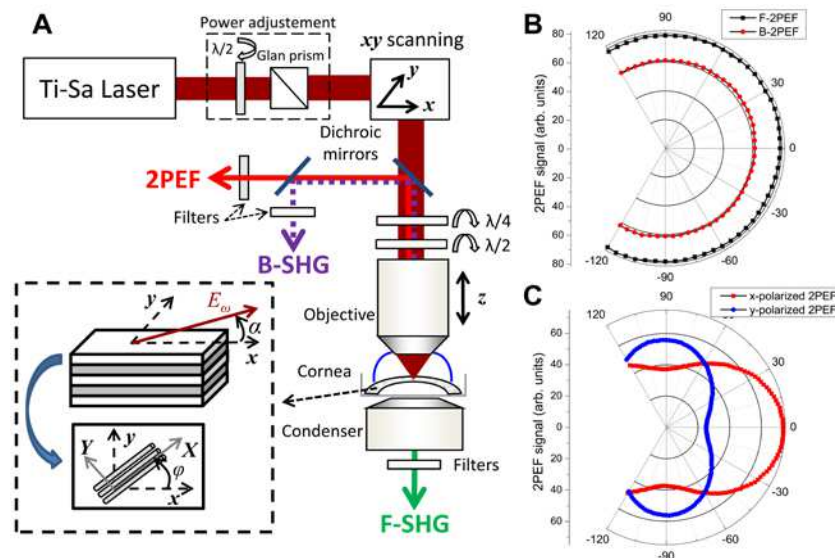


Fig. 1. Experimental setup. (A) Laser scanning microscope with rotating waveplates to control the polarization state of the excitation beam. Orientation of the linearly polarized excitation relative to the cornea morphology in the laboratory frame is indicated in the inset. 2PEF and B-SHG are detected in the backward direction as required in *in vivo* experiments. F-SHG is also detected in *ex vivo* experiments and correlated to polarimetric B-SHG data. (B) Forward and backward 2PEF signals from a fluorescent slab versus orientation of the linearly-polarized excitation, showing variations smaller than 3.2%. (C) Polarization-resolved 2PEF signal from a fluorescent slab versus orientation of the linearly-polarized excitation using polarization sensitive forward detection showing that the maximum 2PEF signal consistently corresponds to x or y polarization of the excitation beam.

information through the whole corneal thickness) axial steps. Laser power at the objective focus was typically 20 to 85 mW.

Polarization-resolved SHG was performed using two motorized achromatic waveplates inserted at the back pupil of the objective (Fig. 1A). A quarter waveplate was first used either to switch to quasi-circular polarization or to correct the 14% ellipticity that is mainly introduced by galvanometric mirrors and dichroic mirror and to obtain a well-defined linear polarization (5% residual ellipticity after correction). A half waveplate was then used to control the orientation of this linear polarization. Polarization-resolved SHG was carefully calibrated as previously reported [26]. We verified that forward and backward 2PEF signals from a fluorescent slab (Chroma), exhibited variations smaller than 3.2% when the linear excitation was rotated (Fig. 1B). The absolute polarization angle of the laser excitation was also verified before each experiment by analyzing the polarization of 2PEF signals using a polarizing beamsplitter and linear polarizers in the forward detection module (Fig. 1C). Circularly polarized excitation was sometimes used to obtain SHG images of collagen lamellae with similar efficiency whatever their orientation in the focal plane. Equivalently, we summed all the SHG images obtained with linearly polarized excitation tuned from  $-90^\circ$  to  $90^\circ$  every  $10^\circ$ .

### *2.2. Human cornea preparation*

The study was conducted according to the tenets of the Declaration of Helsinki and French legislation for scientific use of human corneas, using 7 human corneas, obtained from the French Eye Bank (BFY, Paris, France), which were unsuitable for transplantation [32]. They exhibited an endothelial cell density between 1850 and 2450 cell/mm<sup>2</sup> (mean value: 2130 cell/mm<sup>2</sup>) that is above the viability threshold fixed at 2000 cell/mm<sup>2</sup> for all the corneas except one [32]. They were stored at 31°C in CorneaMax medium (Eurobio, France) until the experiment. A custom-built holder was used for SHG imaging that clamped the sclera and preserved the cornea. This holder was inserted in a Petri dish with refined thickness to optimize the F-SHG signal detection. Corneas were immersed in a storage medium without red phenol (#7002\_WORP, Stem Alpha, France) to prevent tissue drying during SHG imaging. They were slightly edematous as shown by their increased thickness (typically 700  $\mu$ m) compared to physiological corneal thickness (around 500  $\mu$ m).

### *2.3. Ex vivo porcine eyeball imaging*

Freshly enucleated pig eyes were obtained from a local slaughterhouse (Etablissement Guy Harang, France) and stored in Hanks' Balanced Salt Solution (Sigma) until experiment. MPM imaging was performed within 12 hours after the death using a molded agarose gel to hold the eyeball. A gel tear substitute (Lacrigel, Europhtha, Monaco) was used to maintain optical contact between the eye and the immersion objective (1.340 refractive index in the visible range at 22°C as measured with Abbe refractometer).

### *2.4. In vivo rat cornea imaging*

Experiments were conducted in accordance with the Association for Research in Vision and Ophthalmology (ARVO) Statement for the Use of Animals in Ophthalmic and Vision Research. Male three-month old ( $n = 1$ ) and one-year old ( $n = 1$ ) Wistar rats were purchased from Janvier (Le Genest-Saint-Isle, France) and roomed for one week before inclusion in the study. For experiments, rats were anesthetized by intramuscular injection of a mixture of Ketamine (100 mg/kg) and Xylazine (10 mg/kg). The rat was then placed on a plate under the microscope and, after local anesthetic (tetracaine) instillation, the eye was flattened with a coverslip mounted on a custom-built mechanical device. Optical contact was maintained with ophthalmic gel as for porcine eyeballs.

### 3. Polarization-resolved SHG: theoretical background and numerical simulation

#### 3.1. Theoretical background and data processing

The SH response of a medium is characterized by the second order nonlinear susceptibility tensor  $\chi^{(2)}$ . This tensor is obtained as the averaged response of small collagen fibrils aligned in domains within lamellae and it reflects the direction of collagen fibrils in these domains. Assuming that fibrillar collagen exhibits a cylindrical symmetry and that Kleinmann symmetry applies [19,24], it exhibits only two independent components:  $\chi_{xxx}$  and  $\chi_{xyy} = \chi_{xzz} = \chi_{yyx} = \chi_{zxx} = \chi_{yxx} = \chi_{zzx}$ , where  $X$  is the direction of the collagen fibrils (see Fig. 1A). An incident electric field  $\mathbf{E}_0$  then induces the following SH radiation in the fibril frame  $XYZ$ :

$$E_x^{2\omega} \propto [\chi_{xxx} \cos^2(\alpha - \varphi) + \chi_{xyy} \sin^2(\alpha - \varphi)] E_0^2 \quad (1a)$$

$$E_y^{2\omega} \propto [\chi_{xyy} \sin 2(\alpha - \varphi)] E_0^2 \quad (1b)$$

where  $\alpha$  and  $\varphi$  stand for the laser excitation polarization angle and the fibril orientation angle, respectively, with respect to a fixed direction in the laboratory frame (axis  $x$  in Fig. 1A). This formalism is valid because the collagen lamellae are parallel to the surface of the cornea so that the collagen fibrils and the incident electric field are both within the focal plane. The total SH intensity is then given by

$$I^{2\omega} = K \left( \left| \rho \cos^2(\alpha - \varphi) + \sin^2(\alpha - \varphi) \right|^2 + \left| \sin 2(\alpha - \varphi) \right|^2 \right) \quad (2)$$

where  $K$  is a constant merging the squared incident intensity and setup geometrical parameters. Two quantitative parameters appear in this expression: (i) the angle  $(\alpha - \varphi)$  of the laser excitation polarization to the collagen fibrils axis within lamellar domains; (ii) the ratio  $\rho = \frac{\chi_{xxx}}{\chi_{xyy}}$ , which reflects the anisotropy of the nonlinear response of these lamellar domains.

This approach is valid for both B-SHG and F-SHG signals.

Equation (2) can be expressed as a sum of Fourier components  $\cos 2n(\alpha - \varphi)$ , with  $n = 0, 1, 2$  [24,26,33]. This is an efficient way to process the experimental data and determine the SHG anisotropy parameter  $\rho$  even in the presence of optical artifacts due to diattenuation or birefringence in the propagation of the laser excitation [25–27,34]:

$$I^{2\omega} = A \cos 4(\alpha - \varphi) + B \cos 2(\alpha - \varphi) + C \quad (3)$$

As previously derived [26], the SHG anisotropy ratio  $\rho$  is then calculated as

$$\rho = \sqrt{\frac{A+B+C}{A-B+C}} \quad (4)$$

where we have omitted diattenuation correction since there is no diattenuation in the corneal stroma (data not shown). This expression applies even in birefringent media, which may be the case in corneal stroma [35].

Equation (3) was then used to fit the SHG signal in every pixel of the images as a function of the polarization angle of the laser excitation. Image processing was performed automatically using custom-written Matlab script applicable to 3D image stacks with polarimetric information for each pixel (4D data stacks). In order to optimize the signal to noise ratio, the polarization-resolved SHG images were first binned to obtain  $8 \times 8$  to  $13 \times 13 \mu\text{m}^2$  pixel areas. These enlarged regions of interest (ROI) remain smaller than the lamellar domains that extent over  $10 \mu\text{m}$  wide in the anterior stroma to more than  $100 \mu\text{m}$  wide in the

posterior part. Our script then determined for every ROI the angle  $\varphi$  of the collagen fibrils to a reference direction in the laboratory frame, the SHG anisotropy parameter  $\rho$  and the coefficient of determination  $R^2$  which quantifies the goodness of the fitting procedure ( $0 < R^2 < 1$ ).

### 3.2. Numerical simulation of the anisotropy parameter variation with depth

The parameter  $\rho$  is related to the anisotropy of the SH response in *homogenous* lamellar domains composed of aligned nanometric collagen fibrils. Generally speaking, the nonlinear susceptibility formalism is relevant for locally uniform tissue structures. However, two adjacent lamellae with different orientations and consequently different  $\chi^{(2)}$  can contribute together to the SH response when the beam is focused at the interface between them. This configuration occurs at every lamellar interface when scanning along the depth of the cornea. It is expected to induce distortions of the polarimetric diagrams and to hinder the correct determination of the parameters  $\rho$  and  $\varphi$  since the SH response is not uniform throughout the focal volume.

We performed numerical simulation of the depth profile of SHG signals while scanning through an interlamellar interface so as to have a better quantitative understanding of the variation of  $\rho$  and  $\varphi$  in our experimental data. The electric field distribution near the beam focus was calculated using the angular spectrum method [36] for a 1.2 numerical aperture objective (axial FWHM  $\approx 0.9 \mu\text{m}$ ). The second order polarization was calculated at every node of the discretized focal volume, considering two different orientations of the  $\chi^{(2)}$  tensor for the two lamellae, with  $\rho = 1.3$ . The total SH electric fields radiated in different solid angles were then calculated and the total F-SHG intensity was finally obtained for all polarization directions of the excitation beam. These model calculations resulted in distorted polarization diagrams at interfaces due to the contributions of both lamellae. These diagrams were fitted in the same way as our experimental data using Eq. (3). The resulting effective SHG anisotropy parameter  $\rho_{\text{eff}}$  is depicted in Fig. 2A as a function of the angle between two lamellar domains and of the depth position of the lamellar interface within the focal volume.  $\rho_{\text{eff}}$  exhibits a minimum at the interface between two lamellae (for a depth equal to 0 in the simulation), whatever the angle between the two adjacent lamellae. The depth profiles of the effective parameters  $\rho_{\text{eff}}$  and  $\varphi_{\text{eff}}$  for two lamellae at  $60^\circ$  is detailed in Fig. 2B. In addition to the decrease of the  $\rho_{\text{eff}}$  values,  $\varphi_{\text{eff}}$  switches steeply from the direction of the first lamella to the direction of the second one while the goodness of the fit  $R^2$  displays a minimum.

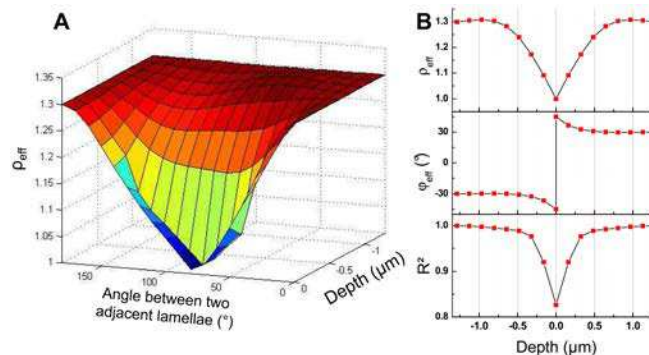


Fig. 2. Numerical simulation of effective SHG anisotropy parameter  $\rho_{\text{eff}}$  across a lamellar interface. (A) Effective SHG anisotropy ratio  $\rho_{\text{eff}}$  obtained by fitting with Eq. (3) simulated polarimetric diagrams with contributions of two adjacent lamellae.  $\rho = 1.3$  within a unique lamella and  $\rho_{\text{eff}}$  varies with the depth of the lamellar interface within the focal volume and with the relative angle of the two lamellae orientations. (B) Simulated depth profiles of the SHG anisotropy ratio ( $\rho_{\text{eff}}$ ), of the orientation of the collagen lamellar domains ( $\varphi_{\text{eff}}$ ) and of the coefficient of determination ( $R^2$ ) for two adjacent lamellae with  $60^\circ$  relative angle.

## 4. Results

### 4.1. Cornea multiphoton imaging

Typical B-SHG and F-SHG images from *ex vivo* human corneas are displayed in Figs. 3A-B. Image stacks in the whole corneal thickness are shown in [Media 1](#). As previously reported, F-SHG images are characterized by striated spatial features, while B-SHG images are nearly homogeneous at the micrometer scale, with speckle-like background interrupted by linear cracks with much smaller signal. Similar features are observed in transverse reconstructions of F-SHG and B-SHG images (Figs. 3C-D and [Media 2](#)). B-SHG images therefore do not directly provide any structural information about the corneal stroma. We have, however, measured that the F-SHG to B-SHG intensity ratio is close to 1 after normalization of both detection channels, so that B-SHG signals are quite large signals. Structural information may therefore be obtained from these signals by performing polarization-resolved SHG microscopy since we expect larger SHG signals when the incident excitation field is aligned with the collagen fibrils. F-SHG and B-SHG polarization-resolved signals are both recorded by rotating the incident polarization as depicted in Fig. 4. We then developed a specific method to process these data based on the tensorial nonlinear optics formalism.

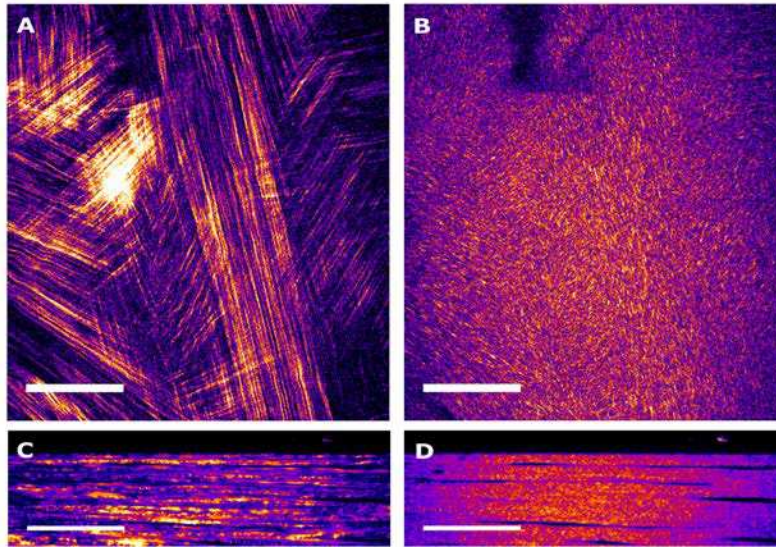


Fig. 3. F-SHG and B-SHG images of posterior stroma from human corneas. (A) F-SHG and (B) B-SHG images obtained as the sum of all the raw images acquired with tunable linear incident polarization (60x 1.2 NA objective, scale bar: 30  $\mu\text{m}$ , false colors) ([Media 1](#)). (C) F-SHG and (D) B-SHG  $xz$  reconstruction from the previous data volume ([Media 2](#)). Striated features (A) and stacked organization (C) are clearly visible in F-SHG images while B-SHG images (C) and (D) are spatially homogenous in.

### 4.2. Determination of fibril orientations

Figure 4 displays typical polarimetric diagrams for the highlighted ROIs in the SHG images. The fits give  $R^2$  values that are close to 1 and consistent for F-SHG and B-SHG signals. It is worth noting that the angle  $\varphi$  (Fig. 4B) corresponds to the orientation of the striated features that appear in F-SHG images (Fig. 4A). It confirms that these striated features reveal the orientation of the collagen fibrils in stromal lamellar domains. In a few ROIs, the  $R^2$  values were lower and fitting F-SHG and B-SHG signals provided different parameters. This discrepancy is related to the specific structures observed in these ROIs. The F-SHG image shows two distinct networks of striated features that seem to be superimposed in the focal volume. It means that the excitation beam was focused at the interface between two lamellae

and that SHG radiation from these two adjacent lamellae was collected together. These two contributions lead to a distortion of the polarization-resolved SHG profile and the fibril orientation cannot be determined unambiguously in such ROIs.

In order to further evaluate the relevance of our method, the angle  $\varphi$  was superimposed on the SHG images, using arrows with length proportional to the  $R^2$  value (Figs. 5A-B). When  $R^2$  values were below an arbitrary threshold (typically 0.7), the results of the fits were discarded. This image processing was performed along the whole depth of the corneal stroma and gave consistent results (Media 3). We observe that the fibrils orientations determined by this approach are (i) the same for F-SHG and B-SHG images although these images exhibit different structures, (ii) in good agreement with the orientations of the micrometric features

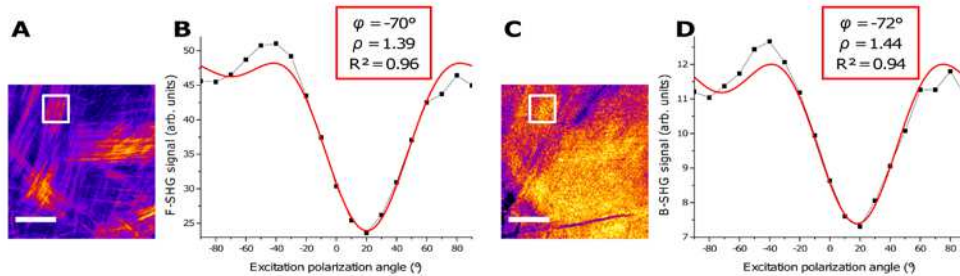


Fig. 4. Polarimetric diagrams from F-SHG and B-SHG images of posterior stroma from human corneas. (A) F-SHG and (C) B-SHG images obtained as the sum of all the raw images acquired with tunable linear incident polarization (20x 0.95 NA objective, scale bar: 50  $\mu\text{m}$ , false colors). (B) F-SHG and (D) B-SHG averaged intensity in the highlighted ROIs versus the angular direction  $\alpha$  of the incident linear polarization. Fits of F-SHG and B-SHG polarimetric diagrams using Eq. (3) (red color) provide the same orientation  $\varphi$  of the collagen lamellar domains and the same SHG anisotropy ratio  $\rho$  with a high coefficient of determination  $R^2$  (see insets).

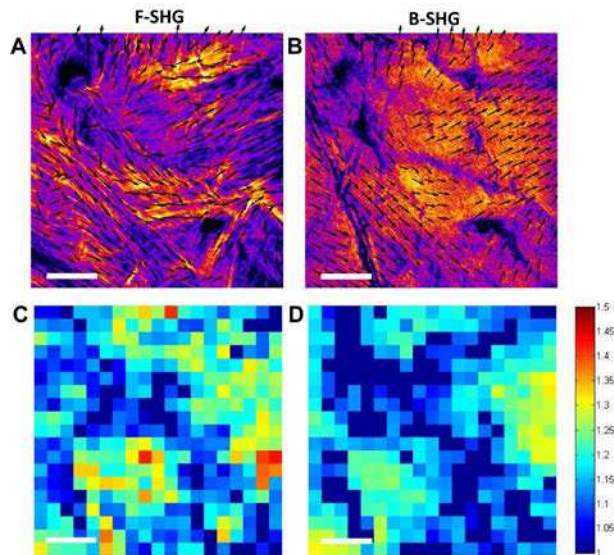


Fig. 5. Orientation maps and SHG anisotropy ratio obtained from polarimetric SHG imaging. (A) F-SHG and (B) B-SHG images of human corneal stroma superimposed with arrows indicating the orientation of collagen fibrils in the lamellar domains calculated from polarimetric diagrams in  $13 \times 13 \mu\text{m}^2$  ROIs using Eq. (3). The arrow lengths scale as  $R^2$  and results are displayed only when  $R^2 > 0.7$ . Maps of the SHG anisotropy ratio  $\rho$  obtained in the same way from (C) F-SHG and (D) B-SHG data. Scale bar: 50  $\mu\text{m}$ . Excitation: 75 mW at 860 nm with a 20x 0.95 NA objective. (Media 3)

revealed in F-SHG images. It shows that polarization-resolved SHG microscopy enables the determination of the collagen fibril orientations within the corneal lamellae using epi-detected signals although raw B-SHG images are spatially homogenous.

The robustness of this approach was characterized as a function of the depth and of the  $R^2$  threshold value (Fig. 6). The greater the  $R^2$  threshold value, the smaller the number of retained ROIs, as expected. The goodness of the fit also gradually deteriorates with depth, which is mainly due to the slight decrease of the SHG signal with depth. While a  $R^2 > 0.9$  threshold appears to be too restrictive because of the weak number of retained ROIs,  $R^2$  thresholds between 0.5 and 0.7 provide a satisfactorily mapping of the angle  $\varphi$  without incongruous results. Using a  $R^2 > 0.7$  threshold, the mean  $R^2$  is  $0.92 \pm 0.07$  (resp.  $0.84 \pm 0.06$ ) and 91% (resp. 63%) of the ROIs are retained for F-SHG images (resp. B-SHG images). It shows that our fitting procedure is robust enough to determine the collagen fibril orientation in the lamellar domains at each depth in the cornea.

This approach also enables the determination of the SHG anisotropy parameter  $\rho$  that shows values between 1.1 and 1.4 in both detection directions (see Figs. 5 C-D).

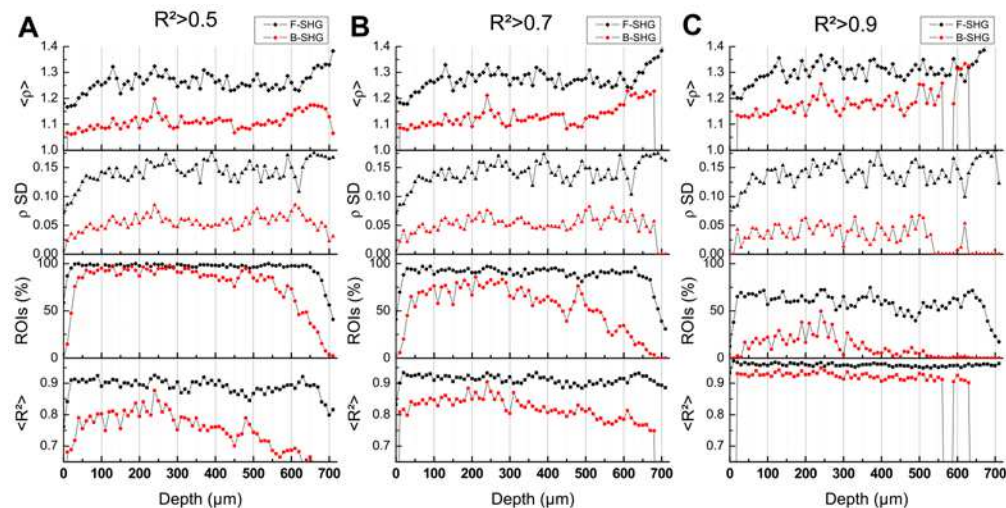


Fig. 6. **Optimization of polarimetric image processing.** Depth profiles of the mean SHG anisotropy ratio ( $\langle \rho \rangle$ ), its standard deviation ( $\rho$  SD), the percentage of retained ROIs above the  $R^2$  threshold (ROIs (%)) and the mean coefficient of determination ( $\langle R^2 \rangle$ ) as obtained from polarization-resolved SHG images, using Eq. (3) with a  $R^2$  threshold equal to (A) 0.5, (B) 0.7 and (C) 0.9.  $13 \times 13 \mu\text{m}^2$  ROIs are processed in  $170 \times 170 \mu\text{m}^2$  F-SHG (black) and B-SHG (red) images over the whole corneal thickness.

#### 4.3. Depth profiles of SHG intensity, SHG anisotropy and lamellar domain orientation

Depth profiles of the SHG signals were measured using a 60x, NA 1.2 objective to increase the axial resolution and to better resolve the lamellae. These measurements were performed in the posterior stroma where the lamellae are thicker and wider. Transverse reconstructions of the anisotropy parameter  $\rho$  show a stacked organization both for F-SHG data (Fig. 7A) and for B-SHG data (Fig. 7B). This feature is better characterized when looking at the depth profiles of the total SHG intensity, of parameter  $\rho$ , of angle  $\varphi$ , and of the  $R^2$  values that are plotted together in Fig. 7C for the  $8.5 \times 8.5 \mu\text{m}^2$  ROI underlined in the image profiles.

Depth profiles of angle  $\varphi$  exhibit plateaus that extend over a few microns and are followed by steep transitions to other plateaus at a quite different angle. This behavior is consistent with the organization of lamellar domains in corneal stroma. The average angular shift between two adjacent lamellae is  $60^\circ \pm 22^\circ$  in this corneal sample, in good agreement with the value determined by electron microscopy from corneal slices [37].

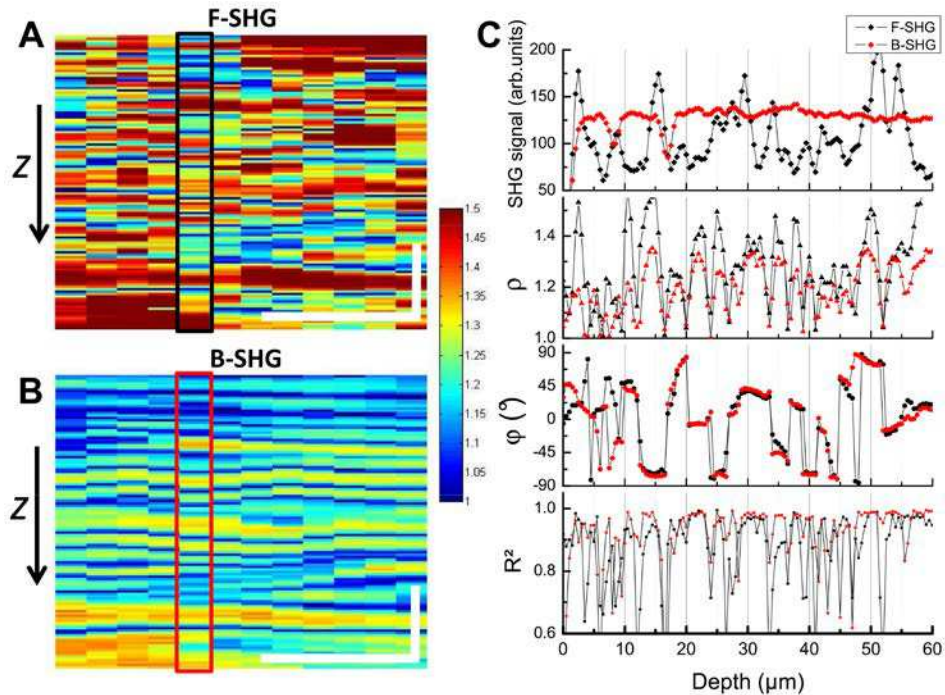


Fig. 7. Depth profiles of polarimetric SHG data in the posterior stroma of a human cornea. SHG anisotropy ratio  $\rho$  along a transverse section obtained from (A) F-SHG and (B) B-SHG polarization-resolved data using  $8.5 \times 8.5 \mu\text{m}^2$  ROIs and  $0.5 \mu\text{m}$   $z$ -steps. Scale bars:  $20 \mu\text{m}$ . Excitation: 20 mW at 860 nm with a  $60\times 1.2$  NA objective. (C) Depth profiles of the total SHG intensity summed for all linear incident polarizations (SHG signal), of the SHG anisotropy ratio ( $\rho$ ), of the orientation of the collagen lamellar domains ( $\varphi$  (°)) and of the coefficient of determination ( $R^2$ ), in forward (black) and backward (red) configurations. A low  $R^2$  threshold (0.5) has been used for this data set.

The SHG anisotropy parameter  $\rho$  also exhibits strong depth variations, with maxima (resp. minima) corresponding to the plateaus (resp. steep variations) in the angle  $\varphi$  profiles. It means that  $\rho$  has local maxima within the lamellae and minima between lamellae. This behavior is consistent for F-SHG and B-SHG data although B-SHG provides slightly smaller  $\rho$  than F-SHG.

The F-SHG intensity profile also reflects the stacked organization of stromal lamellae. Correlation with angle  $\varphi$  profiles show that the intensity maxima are found within the lamellae. This result is in good agreement with previous work that compared SHG and THG intensity depth profiles [15,16]. It is worth noting that the B-SHG intensity profile is much smoother than the F-SHG one. Similarly, transverse reconstructions of B-SHG image stacks do not show the stromal stacked organization observed in F-SHG ones (Media 2). This further substantiates the development of polarization-resolved SHG microscopy for epi-detected imaging.

Finally,  $R^2$  depth profiles exhibit maxima that are correlated with the plateaus of the angle  $\varphi$ , the  $\rho$  maxima, and the F-SHG intensity maxima. The goodness of the fit is therefore higher within the lamellae. Meanwhile, the minima of the  $R^2$  values correlate with the interface between two adjacent lamellae, in agreement with our previous considerations about the fitting accuracy (Fig. 2). Here again, these results are consistent for F-SHG and B-SHG data although B-SHG provides slightly higher  $R^2$  values than F-SHG. This behavior is attributed to the difference in coherence lengths for F-SHG and B-SHG. B-SHG microscopy is characterized by a smaller coherence length and probes smaller axial regions than F-SHG microscopy. It is consequently expected to be sensitive to the interface region between two lamellae over a thinner axial extent.

#### 4.4. Ex vivo eyeball imaging

Intact porcine eyeballs were imaged using polarization-resolved SHG microscopy as a first step toward *in vivo* imaging. Spatially homogeneous B-SHG images were observed as in the *ex vivo* human corneas [11,13,17]. By using the same image processing as above, the orientation and the SHG anisotropy of the different lamellar domains were successfully retrieved for the whole 800  $\mu\text{m}$ -deep cornea (Fig. 8 and Media 4). No comparison was possible with F-SHG signals, which could not be detected in that configuration. Nevertheless, we verified that our results were consistent with physiological data. In particular, the spatial extent of the retrieved lamellar domains was smaller in the anterior stroma than in the posterior one, as expected. Moreover, the high  $R^2$  values certified the goodness of the fitting procedure: using a  $R^2 > 0.7$  threshold, 81% of the binned pixels were retained with  $\langle R^2 \rangle = 0.8 \pm 0.07$ .

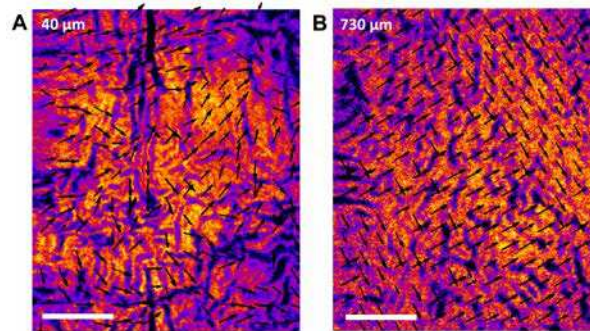


Fig. 8. *Ex vivo* polarization-resolved SHG imaging of intact porcine eyeball. B-SHG images at (A) 40 and (B) 730  $\mu\text{m}$  depth, superimposed with the orientation maps of lamellar domains determined from polarimetric data for  $R^2 > 0.7$ . Scale bar: 50  $\mu\text{m}$ . Excitation: 70 mW at 730 nm with 20x 0.95 NA objective, at 300 kHz pixel rate. Image processing is performed for 13 x 13  $\mu\text{m}^2$  ROIs (Media 4).

#### 4.5. In vivo imaging

Finally, we performed *in vivo* corneal imaging in anesthetized Wistar rat. A custom-built aplanation device was applied to prevent the eye from any movement as in *in vivo* reflectance confocal microscopy. The pixel acquisition rate was also increased to 300 kHz, or typically a

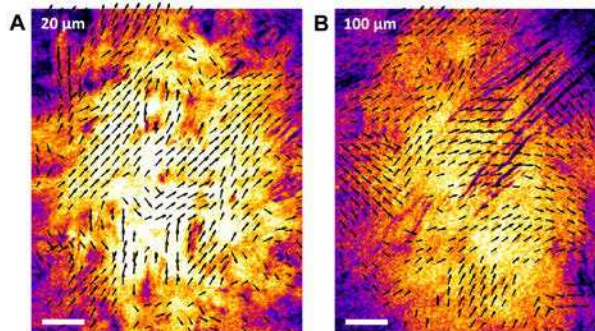


Fig. 9. *In vivo* polarization-resolved SHG imaging from rat cornea. B-SHG images at (A) 20 and (B) 100- $\mu\text{m}$  depth, superimposed with the orientation maps of collagen fibrils in lamellar domains determined from polarimetric data for  $R^2 > 0.7$ . Scale bar: 50  $\mu\text{m}$ . Excitation: 85 mW at 860 nm with a 20x 0.95 NA objective, at 300 kHz pixel rate. Image processing is performed for 13 x 13  $\mu\text{m}^2$  ROIs (Media 5)

few tenths of a second per frame. *In vivo* B-SHG images of the rat cornea were similar to images obtained in *ex vivo* rat eyeball (data not shown). After data processing of SHG polarimetric data, the orientation and the anisotropy of the collagen fibrils in the lamellar domains were successfully retrieved in the whole thickness of the cornea (around 150  $\mu\text{m}$  thick) (Fig. 9 and Media 5) with good statistics: using a  $R^2 > 0.7$  threshold, 70% of the binned pixels were retained with  $\langle R^2 \rangle = 0.85 \pm 0.07$ .

## 5. Discussion

### 5.1. Polarization-resolved SHG of the corneal stroma

In this work, we implemented polarization-resolved SHG imaging to probe the orientation of 30 nm-diameter collagen fibrils in lamellar domains within corneas. The main advantage of our approach is its applicability to both forward and backward detections, opening the way to structural quantitative *in vivo* microscopy. Raw B-SHG images of corneal stroma are indeed spatially homogenous and do not provide any structural information about the collagen lamellae distribution. F-SHG images from excised corneas exhibit striated patterns that reveal the collagen fibril distribution within the lamellae, but they cannot be recorded in *in vivo* configuration. In that context, our approach takes advantage of the enhanced SHG response of collagen fibrils when aligned along the excitation electric field. F-SHG and B-SHG images are recorded for various polarization directions of the laser excitation and suitable data processing retrieves the collagen orientation in every pixel of the SHG images. Fitting of polarimetric data is based on the tensorial formalism of second order nonlinear optics and takes into account possible birefringence of the cornea, which may distort the excitation polarization. The anisotropy of the SHG response in any ROI of the cornea is also measured through the parameter  $\rho$ . It is quite low ( $\rho = 1.1\text{-}1.4$ ), but it appears to be sufficient to determine orientations using Eq. (3), provided that the excitation polarization is well-defined. It is therefore mandatory to correct any ellipticity of the incident beam and to carefully control the rotating angle of the incident polarization.

Our results demonstrate that this new modality is (i) reliable since the retrieved orientation maps are the same for F-SHG and B-SHG images and are in good agreement with the direct visualization of lamellar domain orientations in raw F-SHG images; (ii) robust and efficient since it enables the structural characterization of the lamellar domains along the whole thickness of the corneal tissue with good fitting accuracy (high  $R^2$  values) (Fig. 5 and Media 3); (iii) applicable to intact eyeballs (Fig. 8 and Media 4) and to *in vivo* imaging of rat corneas (Fig. 9 and Media 5).

### 5.2. Comparison between experimental data and numerical simulation

The susceptibility tensor  $\chi^{(2)}$  formally applies to a homogenous medium while the cornea is composed of stacked collagen lamellae. In particular, the SHG collected signals may have contributions from two adjacent lamellae. Accordingly, we observed specific features in the depth profiles of the parameters  $\varphi$ ,  $\rho$  and  $R^2$  obtained when fitting experimental polarization-resolved SHG signals (Fig. 7). Interfaces between lamellae were accurately located thanks to the steep changes of the lamellar domain orientation angle  $\varphi$ . We consistently observed a decrease of  $R^2$  at the same depths. Interestingly, the  $\rho$  depth profiles also exhibited minima at the lamellae interfaces, which means that a heterogeneous SH response in the focal volume results in a lower effective  $\rho$ .

Numerical simulations are in excellent agreement with these experimental results (see Fig. 2B). They fully reproduce the experimental variations of all the parameters through a lamellar interface. Such an excellent agreement cannot be obtained by just averaging the SH anisotropy from two lamellae in the focal volume. Indeed, the peculiar depth profiles we observed experimentally are due to the specific axial phase profile of the excitation beam. Tightly focused beams exhibit a phase shift at the beam focus that is the so-called Gouy phase shift [36]. Practically, the effective phase shift between the front and the back halves of the excitation beam, which illuminate two different lamellae, is about  $\pi/2$ . It means that the

contributions from the two lamellae apart from the interface are in quadrature rather than in phase, so that they contribute independently to the SH response. In other words, they add in an intensity-like manner rather than in a coherent one. This results in a lower effective  $\rho$ .

Finally, our numerical simulations demonstrate that (i) measurement of the orientation of the collagen fibrils in the lamellar domains by polarization-resolved SHG microscopy is robust even near the interface between two lamellae where the polarization diagrams are distorted; (ii) measurement of the SHG anisotropy parameter  $\rho$  must be performed away from any interface in an homogenous region of the cornea to avoid artifacts due to heterogeneities; (iii) variation of the SHG anisotropy parameter  $\rho$  is related to heterogeneities of the fibrillar collagen organization within the focal volume. The latter consideration may be used to study pathological disorders in the cornea, which are characterized by an alteration of the fibril organization inside the lamellae. Measurements of  $\rho$  should also enable monitoring of either corneal reshaping after corneal graft or corneal wounding after any injury.

### 5.3. *In vivo* imaging

Altogether, the main advantage of polarization-resolved SHG microscopy is its applicability to *in vivo* imaging. Our data demonstrates that clear B-SHG images are obtained in anesthetized rats despite the vital movements and that the orientation of the collagen lamellar domains can be retrieved. We estimated that the lateral corneal movements during the acquisition of a polarization-resolved image at a given depth (10 seconds for 18 angular positions) were around a few microns. We therefore processed the SHG data using  $13 \times 13 \mu\text{m}^2$  ROIs that are larger than the corneal movements and small enough compared to the typical lamellae width. Axial movements could not be experimentally determined because B-SHG images were homogenous. However, in case of axial movements, two or more lamellae would contribute to the SHG signal and data fitting would exhibit lower  $R^2$  than for *ex vivo* imaging of immobilized eyeball. Since  $R^2$  are similar in both configurations, we expect that axial movements are marginal and do not disrupt the determination of lamellar domain orientations.

Further *in vivo* studies would require a few improvements of the acquisition conditions. First, the acquisition time could be reduced by degrading the image resolution and increasing the pixel size rather than averaging the signal over large ROIs. The number of polarization-resolved images could also be reduced by using greater angular steps. It would, however, require carefully optimizing the angular step number and total acquisition time to determine the orientation of the lamellar domains with reasonable accuracy [33]. Second, immobilization of the rat eye could be improved by designing a user-friendly system as already used in confocal microscopy; possible artifacts due to fast eye motion could be also corrected by use of suitable image processing to reconstruct undistorted images as reported for confocal microscopy [38]. Third, further studies are necessary to precisely evaluate the maximum power to be used to avoid any tissue damage and ensure cell viability, although no alteration of the stromal collagen was observed during our experiments. Regarding the other ocular tissues such as lens and retina, we expect that our technique is quite safe since the laser is focused in the cornea, similarly to what is routinely performed with pulsed lasers for corneal surgery.

## 6. Conclusion

In this paper, we demonstrated a new method to visualize the structural organization of the cornea without any staining and in an epi-detection configuration that is appropriate for *in vivo* imaging. Our approach merges polarimetric and SHG microscopies to provide quantitative data about the main direction and the heterogeneity of the collagen fibrils distribution. It takes advantage of the high sensitivity of polarimetry for optically anisotropic structures, even below the optical resolution, such as for the 30 nm-diameter stromal collagen fibrils. Using polarization-resolved SHG, we mapped the 3D distribution of collagen lamellae at each depth in human corneas and obtained an excellent agreement with numerical simulations. We also performed *in vivo* SHG imaging of rat corneas and demonstrated that our

approach enables structural imaging of corneal stroma without any labeling and despite the vital movements.

This method opens avenues for preclinical ophthalmological studies, which require dynamic follow-up of corneal lamellar structure in a variety of injuries or pathologies. It should also find applications to *in vivo* diagnosis of human corneal dystrophies or to corneal healing monitoring after keratoplasty or refractive surgery. More generally, epi-detected polarization-resolved SHG imaging can provide quantitative structural information about the 3D organization of collagen fibrils within any tissue. We therefore expect that this new method will extend to other organs and become a new diagnosis tool for collagen remodeling.

### **Acknowledgments**

The authors gratefully acknowledge I. Sourati and P. Sabatier from the “Banque Française des Yeux” for providing the human corneas, X. Solinas and J.-M. Sintès for technical implementation of the setup, K. Plamann, E. Beaurepaire and D. Débarre for fruitful discussions, and M. Zimmerley and F. Hache for critical reading of the manuscript. G. L. was supported by “RTRA-Triangle de la Physique” and “Fondation Berthe Fouassier—Fondation de France.” L. K. was supported by ANR NOUGAT ANR-08-TecSan-012.